

Evaluating the Impact of Semantic Segmentation and Pose Estimation on Dense Semantic SLAM

Suman Raj Bista, David Hall, Ben Talbot, Haoyang Zhang, Feras Dayoub and Niko Sünderhauf

Abstract—Recent Semantic SLAM methods combine classical geometry-based estimation with deep learning-based object detection or semantic segmentation. In this paper we evaluate the quality of semantic maps generated by state-of-the-art class- and instance-aware dense semantic SLAM algorithms whose codes are publicly available and explore the impacts both semantic segmentation and pose estimation have on the quality of semantic maps. We obtain these results by providing algorithms with ground-truth pose and/or semantic segmentation data available from simulated environments. We establish that semantic segmentation is the largest source of error through our experiments, dropping mAP and OMQ performance by up to 74.3% and 71.3% respectively.

I. INTRODUCTION

Semantic scene understanding is an important capability for robotic systems. The ability to determine *what* is *where* within an environment is a fundamental building block of operation. A chief problem within this field of research is semantic simultaneous localization and mapping (SLAM) and, within that, the semantic mapping of objects in 3D space. Utilizing the power of deep learning, there have recently been several influential works in this area capable of providing dense semantic maps [1]–[7]. However, there is limited work in examining the performance of such systems, particularly in understanding the effects of internal components on semantic mapping performance and quality.

In this work, we examine class-aware and instance-aware dense semantic SLAM algorithms to determine what components cause the greatest errors in creating a semantic map. Specifically, we examine the effect of class/instance segmentation and localization on the performance of generating semantic maps. This is a level of analysis for semantic mapping that is rarely seen in the literature.

We are able to analyze sub-components of dense semantic SLAM systems to this level of detail in isolation by using simulated data. While some standard real-world datasets exist such as in [8], [9], we leverage advances in simulated environments for robotics tasks (like [10], [11]) to attain repeatable results in environments with controlled variations. We use the BenchBot framework [12] to gain access to ground-truth instance segmentation, depth, and pose data within a set of simulated environments [13]. By selectively utilizing this ground-truth data within the semantic mapping pipeline, we are able to examine which components have

the highest impact on semantic mapping and compare the different mapping techniques.

The key findings of this paper are as follows:

- Semantic segmentation/object segmentation is the main cause of error in semantic mapping systems;
- Class-aware SLAM systems attain better results than instance-aware systems under ideal conditions due to better data association; and
- Providing perfect segmentation, depth and pose data does not guarantee perfect semantic mapping.

The following section gives an overview of some semantic mapping methods and their evaluation metrics available in the literature. Our approach for the evaluation, along with the methods and evaluation metrics we have used, are described in Section III. Section IV presents and discusses our experimental results. Finally, some concluding remarks are provided in Section V.

II. BACKGROUND LITERATURE

As our work concerns the evaluation of semantic mapping systems, we provide background research in both semantic SLAM/semantic mapping systems and the metrics that are used to evaluate them.

A. Semantic SLAM / Semantic Mapping Systems

Dense SLAM with semantic labels and instance-aware SLAM systems have been developed in recent years by utilizing developments in deep learning, object detection and semantic segmentation. SLAM++ [1], is one of the first RGB-D object-oriented mapping system. Although a pioneering work, SLAM++ requires a database of well-defined 3D models of the objects (full set of object instances with their very detailed geometric shapes) beforehand, which is overly restrictive for widespread application. Comparatively, SemanticFusion [3] builds a dense semantic map by fusing semantic predictions from a convolutional neural network into a dense map built using RGB-D SLAM (ElasticFusion [14]) without needing prior 3D models. Recently [2] built a dense volumetric semantic map incorporating semantic segmentation in the Voxelblox framework proposed by [15]. Both methods are class-aware dense semantic SLAM systems that focus on the general class label given to each pixel in an image rather than individual objects within a scene.

As well as class-aware semantic SLAM systems, some approaches attempt to create semantic maps from instance-aware object detections. MaskFusion [4] builds an instance-aware map by fusing semantic labels from instance-aware

The authors are with Queensland University of Technology (QUT). This research has been conducted by the Australian Research Council Centre of Excellence for Robotic Vision (CE140100016) and supported by the QUT Centre for Robotics. suman.bista@qut.edu.au

semantic segmentation into the RGB-D SLAM system. Fusion++ [16] uses Mask R-CNN [17] instance segmentation to initialize compact per-object Truncated Signed Distance Function (TSDF) reconstructions to build a semantic graph-based map. The consistency of the map is then maintained via loop closure detection, pose-graph optimization and further refinement. An instance-aware semantic map was also developed in [5] by using instance-aware segmentation within RGB images and unsupervised depth segmentation. The work in [6] uses both 2D object detection and 3D geometric segmentation to build an object map. PanopticFusion [7] goes further than just using either class- or instance-aware segmentation, instead utilizing both to build a 3D pantopic map by fusing 2D semantic and instance segmentation outputs refined using dense Conditional Random Field (CRF).

There is also a growing field of works on instance-aware SLAM with sparse representation of the object using geometric primitives like cuboids [18] and quadrics [19]. Both CubeSLAM [18] and QuadricSLAM [19] are monocular object SLAM systems, which rely on the bounding boxes generated by object detection algorithms to estimate the initial cuboid proposal and the quadric parameters respectively. These sparse SLAM systems improve localization accuracy but have their own limitations. In CubeSLAM, vanishing points are also required during cuboid proposal generation, limiting the applicable object categories. The extraction of vanishing points requires the objects to have parallel straight lines on the surface. QuadricSLAM requires the same object to be seen from at least three views to initialize quadric parameters. Furthermore, diverse viewpoints of the objects are required for convergence. The straight-line motions of the robot may not always generate diverse enough viewpoints of objects. Hence, we do not consider these sparse SLAM systems in our evaluation.

B. Evaluation Metrics

Visual SLAM methods are typically evaluated using Absolute Trajectory Error (ATE) and the Relative Pose Error (RPE) [20]. ATE evaluates the global consistency of trajectories by comparing positional offsets between the estimated and the ground-truth trajectories. In contrast, RPE considers the drift of trajectory or local motion errors in the trajectory. Both ATE and RPE are usually expressed as Root-Mean-Square-Error (RMSE) [20], [21] and are beneficial in testing localization accuracy. However, these metrics do not evaluate the semantics or quality of object maps.

With the development of more semantic mapping systems, some approaches have been put forward to evaluate the quality of SLAM maps and the trajectories they produce. SemanticFusion [3] uses pixel average accuracy (percentage of correctly classified pixels) and class average accuracy (the average of the diagonal of the prediction’s normalized confusion matrix). MaskFusion [4] uses 3D error for reconstruction evaluation and Intersection-over-Union (IoU) [22] using the reprojected object mask of the reconstructed 3D model for segmentation evaluation. PanopticFusion [7] uses panoptic quality, segmentation quality and recognition

quality calculated based on IoU over 3D segmentation masks. In QuadricSLAM [19], centroid error is used to measure position quality, and the Jaccard distance ($1 - \text{IoU}$) is used to measure shape quality. The metrics such as accuracy of centroid estimation and IoU evaluate only the spatial quality, whereas semantic maps also have to be evaluated semantically.

Inspired by 2D object detection, the fusion of semantic and spatial analysis is typically done using adaptations of mean average precision (mAP) with IoU in 3D used in place of 2D IoU [18], [23]–[25]. In [5], Average Precision (AP) [22] is computed for each class using an IoU threshold of 0.5 over the predicted 3D segmentation masks. CubeSLAM [18] uses 3D IoU and AP calculated using an IoU threshold of 0.25 for evaluating estimated cuboids. Recently, [13] extends the Probability-based Detection Quality (PDQ) [26] evaluation measure designed for probabilistic object detection to evaluate object-based semantic map. This Object Map Quality (OMQ) evaluation method is used as the metrics in the Scene Understanding Challenge [13]. Since mAP using 3D IoU and OMQ can both evaluate spatial and semantic quality with a single metric, we choose to use them in evaluating the performance of some of the popular semantic mapping algorithms in this work.

III. METHOD OVERVIEW

To establish the impact of semantic segmentation and pose estimation on different semantic SLAM systems, we perform experimental analysis in a set of controlled simulated environments. All experiments were performed on a PC with Intel Core i7 CPU and 16 GB RAM equipped with Nvidia GeForce GTX 1080 GPU having 8 GB graphics memory.

A. Simulation Environments

In this paper, we used the high-fidelity simulator in the BenchBot [12] system to obtain color and depth images, ground-truth poses, and ground-truth class and object segmentation. Example outputs are shown in Fig. 1. The BenchBot system provides access to five simulated indoor environments called miniroom, apartment, house, office and company. Each environment has five variations: base, day, night, day extra and night extra. The variations present changes in both lightning and the objects present within each scene. This system has been primarily designed for the Scene Understanding Challenge and provides ground-truth 3D cuboid maps for 30 classes of object : bottle, cup, knife, bowl, wine glass, fork, spoon, banana, apple, orange, cake, potted plant, mouse, keyboard, laptop, cellphone, book, clock, chair, dining table, couch, bed, toilet, monitor, microwave, toaster, refrigerator, oven, sink, and person [13]. However, we were unable to use all of the objects in the larger environments due to GPU memory requirements of some of the methods being evaluated. As a result, we had to choose a subset of the available simulated environments. We utilize the miniroom and apartment environments as they are small and medium-sized environments respectively. We perform experiments on one day scene (1:base) and one night

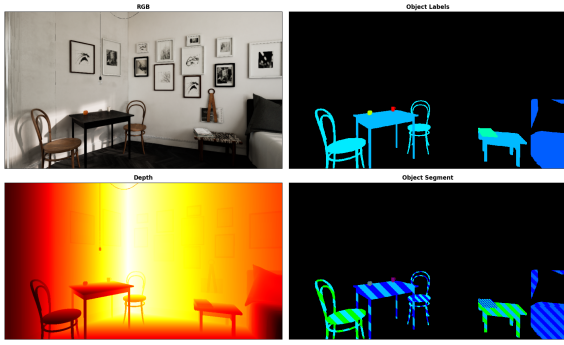


Fig. 1. Image output from the BenchBot simulator: RGB (top-left), Depth (bottom-left), Class Segmentation (top-right), Instance Segmentation (bottom-right). Note that instance segmentation visualization has stripes depicting class and instance id of a given object, but actual output is a single instance value without stripes.

scene (3:night) for both of these environments. Altogether, the algorithms are evaluated in the apartment:1, apartment:3, miniroom:1 and miniroom:3 scenes within BenchBot.

B. Investigated SLAM Systems

Our work examines some of the popular open-source Semantic Mapping/SLAM methods that have publicly available code. We have used the pre-trained models in standard datasets available publicly for object detection and semantic segmentation. Of the available dense class-aware semantic SLAM methods, we examine SemanticFusion (SF) [3] and KimeraSemantics (KS) [2]. For semantic segmentation, we use DilatedNet pertained in the ADE20K dataset [27]. We have specifically chosen this segmentation because of its pre-trained model available in Caffe [28] framework used by SemanticFusion [3]. The instance-aware semantic SLAM approaches analysed in this work are MaskFusion (MF) [4] and Voxblox++ (Vpp) [5]. Fusion++ [16] was not used due to an absence of publicly available code. For these, the instance-level segmentation is provided by Mask R-CNN [17] pre-trained on the MS COCO dataset [29]. For all methods, the estimated poses are obtained from ElasticFusion [14] when ground-truth poses are not used.

1) *SemanticFusion (SF)* [3]: SemanticFusion combines semantic predictions from deep-learned networks with ElasticFusion [14]. ElasticFusion is a real time RGB-D SLAM that provides dense correspondences between frames and a globally consistent map of fused surfels. The semantic predictions consist of a set of per-pixel class probabilities. The class probability distribution for each surfel is updated using Bayesian update from the semantic predictions and correspondences provided by the SLAM system. The semantic predictions in the map are further improved using fully-connected CRF regularization. We have used publicly available SemanticFusion code [30], which uses the Caffe framework [28] for semantic predictions. The original code uses a pre-trained model in the NYUv2 dataset, consisting of only 12 classes that do not cover all the classes required for our tests. Consequently, we used the semantic predictions from DilatedNet, which is pre-trained on the ADE20K dataset [27] and also available in Caffe. To make

[27] compatible with SemanticFusion, we added a softmax layer after the final up-sampled fully connected layer, which outputs per-pixel class probabilities. When using ground-truth segmentation from Benchbot, we generate per-pixel class probability from ground-truth masks where the class probability for the ground-truth class is assigned as 1.0.

2) *MaskFusion (MF)* [4]: MaskFusion uses the object masks obtained from instance-level semantic segmentation to create an instance-aware semantic map, with each object in the 3D map represented as a set of surfels. The object mask is derived by combining the geometric segmentation with the instance-level semantic segmentation. The geometric segmentation is obtained from the analysis of depth discontinuities and surface normals, whereas the instance-level semantic segmentation is obtained either from Mask R-CNN [17] (pre-trained on the MS COCO dataset [29]) or from BenchBot’s ground-truth segmentation. We used the code of MaskFusion available in [31], which requires a high-end GPU with enough memory to store multiple models simultaneously for smooth real-time performance. Therefore, the GPU memory limited the size of the environment and the number of the objects that could be mapped successfully.

3) *Voxblox++ (Vpp)* [5]: Voxblox++ creates volumetric object-centric maps incrementally. The frame-wise instance segmentation is obtained by combining the unsupervised geometric segmentation of depth images with supervised semantic object predictions from RGB. The data association strategy tracks the individual predicted instances across multiple frames. Finally, observed surface geometry and semantic information are fused into a global TSDF map volume. We have used the code of Voxblox++ available in [32], where [33] is used for depth segmentation and either Mask R-CNN (pre-trained in the MS COCO dataset) or BenchBot’s ground-truth segmentation is used for instance segmentation. Except for the Mask R-CNN component, all other stages of Voxblox++ can run online on a CPU.

4) *KimeraSemantics (KS)* [2]: KimeraSemantics uses semantically labeled images to produce a lightweight metric-semantic mesh model of the environment. The semantic labels obtained from 2D semantic segmentation are attached to each point in the 3D point cloud, which is obtained from RGB-D or dense stereo. Next, bundled raycasting from Voxblox [15] is applied, with the label probabilities built from the frequency of the observed labels in each bundle. Bayesian updates are then used to update the label probabilities at each voxel while traversing the voxels along the ray. TSDF is used to filter out noise and extract the global mesh. We used the code of KimeraSemantics available in [34], where 2D semantic segmentation is obtained from DilatedNet (pre-trained on the ADE20K dataset) or BenchBot’s ground-truth segmentation. This method is modular and can run in real-time on a CPU.

To evaluate against the 3D object cuboid ground-truth maps supplied by BenchBot, we require each tested method to output instance-wise, semantically labeled, axis-aligned object cuboids. The global maps obtained from SemanticFusion and KimeraSemantics give 3D semantic point clouds at

the class level rather than the instance level. The instance point cloud for each class is extracted by segmenting the point cloud of the corresponding class based on the Euclidean distance using MATLAB’s `pcsegdist` function [35]. MaskFusion and Voxelbox++ already give point clouds of the object instances in the global map frame. The point cloud of each object instance is used to obtain axis-aligned cuboids in the world-coordinate frame that can be used within the evaluation.

C. Evaluation Metrics

Our work focuses on evaluating the semantic maps produced by semantic SLAM systems by comparing estimated object cuboids with their ground-truth counterparts. To perform our analysis, we use two metrics:

- 1) mean Average Precision (mAP) [22], [29] calculated based on the IoU of cuboids, and
- 2) Object Map Quality (OMQ) [13].

Calculating the 3D IoU between ground-truth cuboids and those produced by the Semantic SLAM systems is a core component to both measures. Given ground-truth cuboids and estimated cuboids axis-aligned in world coordinate frame parameterized by a centroid (x, y, z) and the cuboids full extent (l, b, w) , we can compute IoU in 3D as follows:

$$IoU_{3D} = \frac{V_{overlap}}{V_{gt} + V_{est} - V_{overlap}}, \quad (1)$$

where V_{gt} is the volume of the ground-truth cuboid, V_{est} is the volume of the estimated cuboid, $V_{overlap}$ is the overlapped volume as shown in Fig. 2.

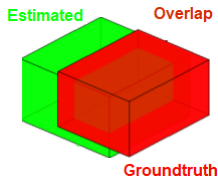


Fig. 2. Visualization of calculating IoU in 3D.

Each of the evaluation metrics then has its own set of implementation details, which are outlined in the following two paragraphs:

1) *mAP using 3D IoU*: We calculate mAP using 3D IoU for IoU thresholds 0.25 to 0.95 at interval of 0.05 (i.e. 0.25 : 0.05 : 0.95) similar to [36]. Mapped cuboids are considered true positives (TP) if: a) the IoU of the estimated and ground-truth cuboid exceeds the threshold, and b) both estimated and ground-truth objects share the same class. To find the closest match in the ground-truth list, we sort all the detections belonging to the same class in descending order of the confidence score and search for the ground truth object in the same class with the highest IoU. Precision-recall (PR) curves [22] for each class are calculated at each of these 15 IoU thresholds. A PR curve is then created using the average precision swept across all classes and IoU thresholds. Lastly, the final mAP score for the scene is given as the average of all of these precision values. We denote it by mAP_{3D} . mAP is also calculated for the thresholds 0.25 and 0.5 for

the scene as is done in [36], and denoted by mAP_{3D}^{25} and mAP_{3D}^{50} respectively.

2) *OMQ*: Adapted from the probability-based detection quality (PDQ) evaluation measure [26], OMQ [13] is a new measure for evaluating 3D object maps. A pairwise object quality (pOQ) is calculated between each object in the proposed map and each ground-truth object in the ground-truth map. The pOQ score is the geometric mean of spatial quality (Q_{Sp}) and label quality (Q_L). For the i^{th} proposed object (O_i) and j^{th} ground-truth object (\hat{O}_j), pOQ is defined as

$$pOQ(O_i, \hat{O}_j) = \sqrt{Q_{Sp}(O_i, \hat{O}_j) \cdot Q_L(O_i, \hat{O}_j)}. \quad (2)$$

Q_{Sp} is simply the IoU score in 3D between ground-truth and proposed object cuboids. Q_L is the probability given to the correct class. Once all pairwise scores are calculated, objects in the proposed map are optimally assigned to objects in the ground-truth map. From this, a list of true positive quality scores with non-zero quality assignments (\mathbf{q}_{TP}), and the number of true positives (n_{TP}), false negatives (n_{FN}), and false positives (n_{FP}) are obtained. In order to weigh overconfident false positives as worse than low-confidence false positives, a list of false positive costs (\mathbf{c}_{FP}) for all false positives is calculated. False positive cost is simply the maximum label probability given to a non-background class label. The final OMQ score is defined as

$$OMQ = \frac{\sum_{i=1}^{n_{TP}} \mathbf{q}_{TP}(i)}{n_{TP} + n_{FN} + \sum_{i=1}^{n_{FP}} \mathbf{c}_{FP}(i)}. \quad (3)$$

D. Testing Scenarios

For evaluation, we compared the estimated cuboid map generated by the methods mentioned earlier against the ground-truth cuboid map provided by the BenchBot in the following scenarios:

- i) *Case I*: Using all ground-truth data obtained from [12], i.e., ground-truth poses and ground-truth segmentation or ground-truth object masks. This case is the ideal scenario that uses perfect localization and detection that serves as a baseline for the given method.
- ii) *Case II*: Using ground-truth poses and estimated class-based [27] or object-based [17] segmentation using deep neural networks. This case is used to evaluate mapping performance in the simulated environment using the network pre-trained on real-world data within a perfect localization scenario.
- iii) *Case III*: Using estimated pose from dense RGB-D SLAM [14] and ground-truth segmentation or ground-truth object masks. This case is used to evaluate how much the map quality is affected using the estimated pose when detections are perfect.
- iv) *Case IV*: Using estimated pose [14] and estimated segmentation [27] or object masks [17]. This case is used to evaluate how much the map quality is affected in the realistic robotic scenario using estimated poses and detections.

IV. EXPERIMENTS AND RESULTS

Tables I, III, IV and V present the evaluation scores using metrics outlined in Sect. III-C for Cases I, II, III and IV respectively. The considered methods SemanticFusion, MaskFusion, Voxelbox++ and KimeraSemantics are denoted by SF, MF, Vpp and KS respectively. We denote environments apartment:1, apartment:3, miniroom:1 and miniroom:3 as ap1, ap3, mr1 and mr3 respectively. The root mean square trajectory error between the estimated pose obtained from [14] and the ground-truth pose are presented in Table II. We use Absolute Trajectory Error (ATE) and Relative Pose Error (RPE) to measure the trajectory error.

The metrics in Tables I, III, IV and V are as follows: mAP_{3D} is the average mAP using 3D IoU for IoU threshold 0.25 to 0.95 at the interval of 0.05, mAP_{3D}^{25} is the average mAP using 3D IoU threshold of 0.25, mAP_{3D}^{50} is the average mAP using 3D IoU threshold of 0.5, OMQ is Object Map Quality score, mPOQ is the average pairwise quality of true positives, mLQ is the average label quality of true positives, and mFPQ is the average spatial quality (3D IoU) of true positives. The metrics rmAP, rAP25, rAP50, and rOMQ are the ratio of mAP_{3D} , mAP_{3D}^{25} , mAP_{3D}^{50} , and OMQ respectively with their corresponding score calculated using all ground-truths.

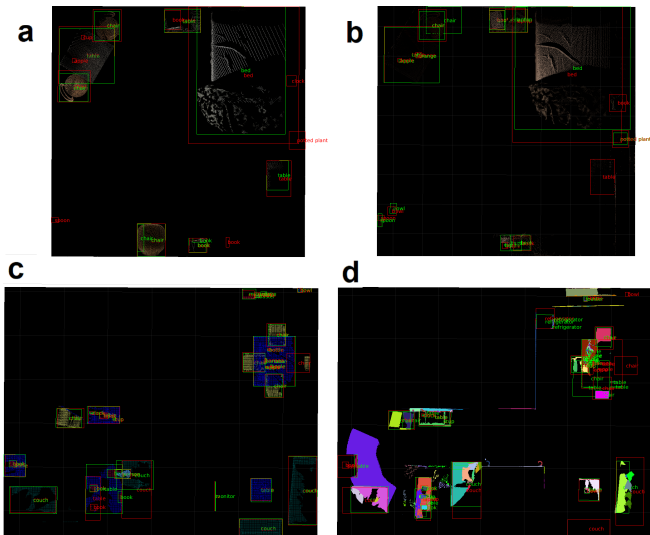


Fig. 3. Object Maps using all ground-truths. **a** MaskFusion on miniroom:1, **b** SemanticFusion on miniroom:3, **c** KimeraSemantics on apartment:1, and **d** Voxelbox++ on apartment:3. Ground-truth cuboids are shown in red. Estimated Cuboids are shown in green.

We summarize the quantitative results of our experiments in Figs. 4, 5, and 6. Note that in Fig. 5 we show the ratio of evaluation scores when compared to the best-case scenario (*Case I*). Our results show that in ideal conditions (*Case I*), methods that use class-aware segmentation like KS and SF perform better than the methods that use instance-aware segmentation like Vpp and MF because some objects are not appropriately associated in a 3D map when seen from different views. This is shown in detail in Fig. 3. In Fig. 3a, we see a chair and book, and in Fig. 3d, we see a refrigerator, table and chair that do not have good data

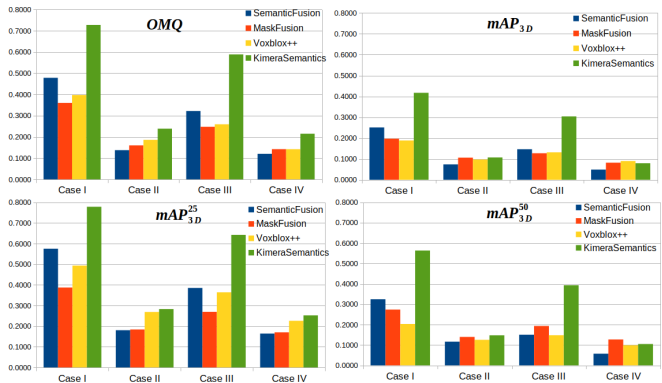


Fig. 4. OMQ and mAP scores based on IoU in 3D.

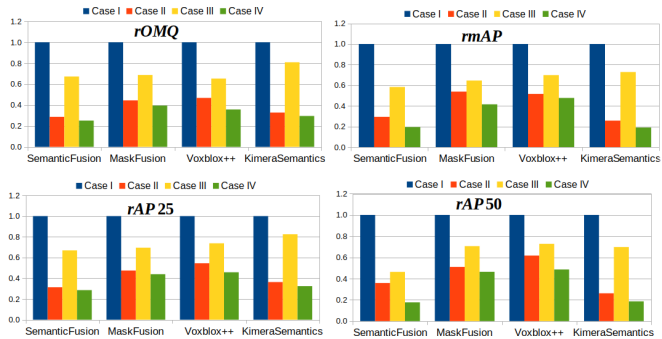


Fig. 5. Ratio of OMQ and mAP with their corresponding score calculated for *Case I*.

association when using MF and Vpp respectively. The same object has been detected as a few fragmented cuboids. One of these fragments may be taken as a true positive during the evaluation, while the rest are considered false positives. In SF and KS, object instances are extracted from the global semantic map after the mapping is completed, unlike in MF and Vpp, where object instances in the map are built incrementally. Hence, SF and KS seem to have a better data association for the objects in the global map. Even when we use all ground-truth data (*Case I*), the resulting map is not perfect. Fig. 6 presents detailed analysis with different IoU thresholds and breakdown of errors. Even when the localization error and background false positives are removed, the mAP is not perfect. The main reason for this is that objects or their parts are missed during the creation of the semantic 3D model using the 2D object mask or segmentation and the depth image. In order to filter out noise, these methods ignore objects a certain distance away or of a certain size. Furthermore, some objects get missed or only the parts of them get mapped because they have been seen from limited views or very few times or both. In Fig. 4 mAP scores and in Fig. 6 area under the PR curve decrease with an increase in the IoU threshold, which signifies that only certain parts of the object get mapped. Since we have considered that the object is fully confident to belong to a particular class while building the object maps, the OMQ score solely depends upon the spatial quality, i.e., IoU in 3D. When we look at Fig. 4, KS creates better maps than other methods based on OMQ and mAP metrics because the 3D global mesh produced by KS is very accurate [2].

Method	Scene	mAP _{3D}	mAP _{3D} ²⁵	mAP _{3D} ⁵⁰	OMQ	mPOQ	mLQ	mSQ	mFPQ
Semantic Fusion (SF)	apartment:1 (ap1)	0.2641	0.5538	0.3772	0.5450	0.6812	1.0	0.4882	1.00
Mask Fusion (MF)		0.2004	0.2671	0.2671	0.3993	0.8486	1.0	0.7273	0.00
Voxblox++ (Vpp)		0.1268	0.3848	0.0830	0.5108	0.6385	1.0	0.4502	1.00
Kimera Semantics (KS)		0.3804	0.7402	0.4947	0.7473	0.7473	1.0	0.5942	1.00
Semantic Fusion (SF)	apartment:3 (ap3)	0.1406	0.3986	0.1944	0.3568	0.5946	1.0	0.4062	0.00
Mask Fusion (MF)		0.0626	0.2250	0.0750	0.2103	0.7011	1.0	0.5159	0.00
Voxblox++ (Vpp)		0.2024	0.4521	0.2595	0.2827	0.6597	1.0	0.4774	0.00
Kimera Semantics (KS)		0.4434	0.8167	0.6037	0.7461	0.7718	1.0	0.6202	1.00
Semantic Fusion (SF)	miniroom:1 (mr1)	0.2272	0.5926	0.2407	0.5532	0.7235	1.0	0.5512	0.00
Mask Fusion (MF)		0.2401	0.3611	0.3333	0.5225	0.6345	1.0	0.4534	0.00
Voxblox++ (Vpp)		0.1951	0.4815	0.2222	0.5316	0.6645	1.0	0.4742	1.00
Kimera Semantics (KS)		0.3844	0.7407	0.5185	0.7607	0.7607	1.0	0.6108	1.00
Semantic Fusion (SF)	miniroom:3 (mr3)	0.3717	0.7576	0.4848	0.4589	0.6555	1.0	0.4863	0.00
Mask Fusion (MF)		0.2852	0.6970	0.4192	0.3082	0.7266	1.0	0.5807	0.00
Voxblox++ (Vpp)		0.2296	0.6566	0.2475	0.2640	0.5029	1.0	0.3028	0.00
Kimera Semantics (KS)		0.4606	0.8182	0.6364	0.6563	0.7735	1.0	0.6313	0.00
Semantic Fusion (SF)	Average (Avg.)	0.2509	0.5756	0.3243	0.4785	0.6637	1.0	0.4830	0.25
Mask Fusion (MF)		0.1971	0.3876	0.2737	0.3601	0.7277	1.0	0.5693	0.00
Voxblox++ (Vpp)		0.1885	0.4937	0.2031	0.3973	0.6164	1.0	0.4261	0.50
Kimera Semantics (KS)		0.4172	0.7790	0.5633	0.7276	0.7633	1.0	0.6141	0.75

TABLE I

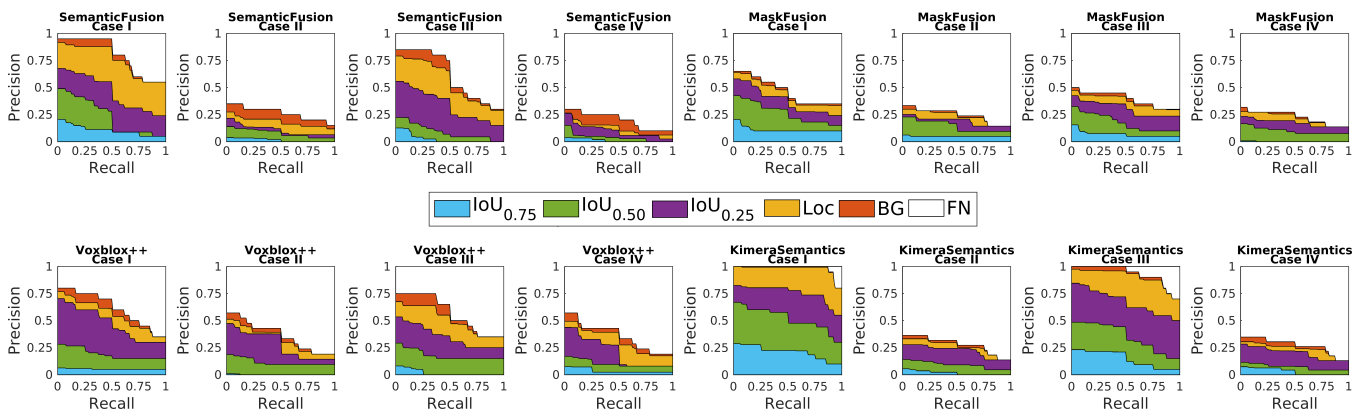
USING ALL GROUND-TRUTH DATA OBTAINED FROM [12] (*Case I*).

Fig. 6. Precision-Recall (PR) Curves. $\text{IoU}_{0.75}$, $\text{IoU}_{0.50}$, and $\text{IoU}_{0.25}$ are PR curves at IoU thresholds 0.75, 0.50, and 0.25 respectively over all four scenes. Loc is the PR curve at IoU threshold 0.10 where localization errors are ignored while considering duplicate detections. BG is the PR curve at IoU threshold 0.10 after all background false positives are removed. FN is the PR curve after all errors are removed. (Note: the plots are inspired from [36].)

When examining *Case II*, which utilizes estimates of class- and instance-aware segmentation, we notice that the performance of all methods drops dramatically. The mAP and OMQ performances in this scenario drop by up to 74.3% and 71.3% respectively under this single condition. The performance drop is higher for SF and KS than MF and Vpp, which we ascribe to the fact that Mask R-CNN produces more accurate object-wise segmentation masks than the class-wise segmentation masks of DilatedNet. This dramatic decrease in performance shows that accurate segmentation of classes/objects is a major limitation in attaining accurate semantic masks when using the current state-of-the-art semantic SLAM systems.

If instead we use ground-truth segmentation and instead estimate robot pose within the Semantic SLAM system (*Case III*), we notice less of a reduction in semantic mapping performance. There is still a decrease in performance which can be attributed to the trajectory errors that we present in Table II. When comparing the orange and yellow bars in Fig. 5 (*Case II* and *Case III* respectively), it is clear that

Scene	Trajectory Length (m)	ATE (m)	RPE Translation (m)	RPE Rotation (deg)
ap1	16.1973	0.0671	0.0056	0.6464
ap3	19.6031	0.0123	0.0051	0.1961
mr1	3.5404	0.0540	0.0185	1.3724
mr3	2.1417	0.0395	0.0109	0.3698
Avg.	10.3706	0.0432	0.0100	0.6462

TABLE II

RMSE ATE AND RPE ERROR BETWEEN GROUND TRUTH TRAJECTORY AND ESTIMATED TRAJECTORY OBTAINED FROM [14].

segmentation error contributes more to low scores than the pose estimation error. The mAP and OMQ performances in this scenario drop by up to 41.7% and 34.7% respectively.

When we consider the case where both segmentation and pose are estimated (*Case IV*), shown in green (Fig. 5), we see the drop in performance does not far exceed that of *Case II* in orange. The average performance drops to 0.401, 0.664, and 0.319 for Cases *II*, *III* and *IV* respectively compared to *Case I* based on mAP. The average performance drops to 0.382, 0.705, and 0.325 respectively based on OMQ. *Case IV* is the scenario most equivalent to the real robotic scenario but in a simulated environment. From our results, we conclude that

Method	Scene	mAP _{3D}	mAP _{3D} ²⁵	mAP _{3D} ⁵⁰	OMQ	mPOQ	mLQ	mSQ	mFPQ	rmAP	rAP25	rAP50	rOMQ
SF	ap1	0.0644	0.1346	0.0788	0.1330	0.6652	1.0	0.4649	0.00	0.2439	0.2431	0.2089	0.2441
MF		0.1292	0.2089	0.1768	0.2430	0.8263	1.0	0.6907	0.00	0.6446	0.7821	0.6618	0.6086
Vpp		0.0920	0.3083	0.0786	0.2421	0.6572	1.0	0.5161	0.00	0.7256	0.8014	0.9462	0.4740
KS		0.0618	0.1543	0.0971	0.2576	0.6583	1.0	0.4739	0.00	0.1626	0.2084	0.1964	0.3447
SF	ap3	0.0475	0.1472	0.0375	0.1439	0.5515	1.0	0.3558	0.00	0.3381	0.3693	0.1929	0.4033
MF		0.0260	0.0556	0.0382	0.0942	0.5518	1.0	0.3824	0.00	0.4157	0.2469	0.5093	0.4479
Vpp		0.0634	0.2181	0.0549	0.1356	0.5086	1.0	0.3206	0.00	0.3132	0.4824	0.2114	0.4797
KS		0.0530	0.1806	0.0417	0.1949	0.6146	1.0	0.4204	0.00	0.1195	0.2211	0.0690	0.2612
SF	mr1	0.0860	0.1975	0.1975	0.1405	0.5018	1.0	0.3399	0.00	0.3786	0.3333	0.8205	0.2540
MF		0.1580	0.2593	0.2222	0.1575	0.7089	1.0	0.5297	0.00	0.6581	0.7179	0.6667	0.3015
Vpp		0.0993	0.2012	0.2012	0.2110	0.5803	1.0	0.3871	0.00	0.5089	0.4179	0.9056	0.3970
KS		0.1654	0.4259	0.2593	0.2856	0.6784	1.0	0.4809	0.00	0.4304	0.5750	0.5000	0.3755
SF	mr3	0.0970	0.2424	0.1515	0.1324	0.6288	1.0	0.4543	0.00	0.2609	0.3200	0.3125	0.2885
MF		0.1111	0.2121	0.1212	0.1452	0.6242	1.0	0.4479	0.00	0.3896	0.3043	0.2892	0.4709
Vpp		0.1343	0.3485	0.1667	0.1554	0.4557	1.0	0.2586	0.00	0.5850	0.5308	0.6735	0.5885
KS		0.1483	0.3712	0.1919	0.2165	0.6341	1.0	0.4492	0.00	0.3220	0.4537	0.3016	0.3299
SF	Avg.	0.0737	0.1805	0.1163	0.1375	0.5868	1.0	0.4037	0.00	0.2939	0.3135	0.3587	0.2873
MF		0.1061	0.1840	0.1396	0.1600	0.6778	1.0	0.5127	0.00	0.5383	0.4747	0.5101	0.4443
Vpp		0.0972	0.2690	0.1253	0.1860	0.5504	1.0	0.3706	0.00	0.5160	0.5449	0.6172	0.4682
KS		0.1071	0.2830	0.1475	0.2386	0.6463	1.0	0.4561	0.00	0.2568	0.3633	0.2618	0.3280

TABLE III

USING GROUND-TRUTH POSE FROM [12] AND ESTIMATED SEGMENTATION [27] OR OBJECT MASKS [17] (Case II).

Method	Scene	mAP _{3D}	mAP _{3D} ²⁵	mAP _{3D} ⁵⁰	OMQ	mPOQ	mLQ	mSQ	mFPQ	rmAP	rAP25	rAP50	rOMQ
SF	ap1	0.1586	0.4452	0.1417	0.1672	0.5853	1.0	0.3536	0.00	0.6004	0.8040	0.3756	0.3068
MF		0.1354	0.2420	0.1705	0.2632	0.7020	1.0	0.5000	0.00	0.6755	0.9057	0.6384	0.6592
Vpp		0.0490	0.2655	0.0274	0.2219	0.5446	1.0	0.3388	0.00	0.3869	0.6900	0.3297	0.4343
KS		0.2683	0.6619	0.3402	0.4398	0.6597	1.0	0.4709	0.00	0.7055	0.8942	0.6876	0.5885
SF	ap3	0.0958	0.1890	0.1500	0.2637	0.5670	1.0	0.3768	0.00	0.6812	0.4742	0.7714	0.7393
MF		0.0429	0.2155	0.0472	0.1881	0.6268	1.0	0.4369	0.00	0.6862	0.9577	0.6296	0.8941
Vpp		0.1547	0.3535	0.1868	0.2780	0.6115	1.0	0.4344	0.00	0.7645	0.7819	0.7198	0.9831
KS		0.3324	0.6500	0.3764	0.6676	0.7153	1.0	0.5545	1.00	0.7496	0.7959	0.6235	0.8948
SF	mr1	0.0383	0.2407	0.0370	0.4416	0.6992	1.0	0.5231	0.00	0.1685	0.4062	0.1538	0.7982
MF		0.1043	0.2870	0.2222	0.2874	0.8623	1.0	0.7448	1.00	0.4344	0.7949	0.6667	0.5501
Vpp		0.1280	0.3025	0.1852	0.3840	0.5761	1.0	0.3878	0.00	0.6561	0.6282	0.8333	0.7224
KS		0.2490	0.4630	0.3333	0.6880	0.7339	1.0	0.5632	0.00	0.6478	0.6250	0.6429	0.9044
SF	mr3	0.2929	0.6667	0.2727	0.4148	0.6221	1.0	0.4389	0.00	0.7880	0.8800	0.5625	0.9038
MF		0.2263	0.3333	0.3333	0.2513	0.6462	1.0	0.4747	0.00	0.7934	0.4783	0.7952	0.8153
Vpp		0.1946	0.5354	0.1919	0.1539	0.4345	1.0	0.2402	0.00	0.8475	0.8154	0.7755	0.5829
KS		0.3655	0.7955	0.5227	0.5592	0.6590	1.0	0.4829	0.00	0.7935	0.9722	0.8214	0.8520
SF	Avg.	0.1464	0.3854	0.1504	0.3218	0.6184	1.0	0.4231	0.00	0.5835	0.6695	0.4636	0.6726
MF		0.1272	0.2695	0.1933	0.2475	0.7093	1.0	0.5391	0.25	0.6456	0.6953	0.7064	0.6873
Vpp		0.1316	0.3642	0.1478	0.2594	0.5417	1.0	0.3503	0.00	0.6983	0.7377	0.7280	0.6530
KS		0.3038	0.6426	0.3932	0.5887	0.6920	1.0	0.5179	0.25	0.7282	0.8249	0.6979	0.8090

TABLE IV

USING GROUND-TRUTH SEGMENTATION OR OBJECT MASKS FROM [12] AND ESTIMATED POSE FROM [14] (Case III).

Method	Scene	mAP _{3D}	mAP _{3D} ²⁵	mAP _{3D} ⁵⁰	OMQ	mPOQ	mLQ	mSQ	mFPQ	rmAP	rAP25	rAP50	rOMQ
SF	ap1	0.0542	0.1429	0.0713	0.0891	0.5167	1.0	0.2720	0.00	0.2050	0.2580	0.1891	0.1635
MF		0.0776	0.2000	0.0964	0.1928	0.6939	1.0	0.5326	0.00	0.3874	0.7487	0.3610	0.4827
Vpp		0.0824	0.2430	0.0762	0.0980	0.4760	1.0	0.2736	0.00	0.6500	0.6316	0.9176	0.1918
KS		0.0355	0.1348	0.0515	0.2090	0.6531	1.0	0.4465	0.00	0.0934	0.1821	0.1041	0.2797
SF	ap3	0.0479	0.1233	0.0521	0.1243	0.5386	1.0	0.3385	0.00	0.3407	0.3094	0.2679	0.3484
MF		0.0239	0.0556	0.0330	0.0928	0.5434	1.0	0.3737	0.00	0.3817	0.2469	0.4398	0.4411
Vpp		0.0582	0.1486	0.0562	0.1548	0.4764	1.0	0.3030	0.00	0.2875	0.3287	0.2168	0.5476
KS		0.0475	0.1847	0.0417	0.1884	0.6230	1.0	0.4309	0.00	0.1071	0.2262	0.0690	0.2525
SF	mr1	0.0173	0.1481	0.0000	0.1397	0.5121	1.0	0.3133	0.00	0.0761	0.2500	0.0000	0.2525
MF		0.1105	0.2130	0.1667	0.1574	0.7083	1.0	0.5318	0.00	0.4602	0.5897	0.5000	0.3013
Vpp		0.0794	0.1493	0.1111	0.2147	0.6440	1.0	0.4486	0.00	0.4068	0.3101	0.5000	0.4038
KS		0.1321	0.3642	0.1790	0.2723	0.6467	1.0	0.4333	0.00	0.3437	0.4917	0.3452	0.3580
SF	mr3	0.0758	0.2424	0.1061	0.1275	0.5421	1.0	0.3686	0.00	0.2038	0.3200	0.2187	0.2779
MF		0.1152	0.2121	0.2121	0.1259	0.5413	1.0	0.3399	0.00	0.4038	0.3043	0.5060	0.4084
Vpp		0.1394	0.3636	0.1515	0.1004	0.4866	1.0	0.2792	0.00	0.6070	0.5538	0.6122	0.3803
KS		0.1019	0.3258	0.1465	0.1900	0.5565	1.0	0.3563	0.00	0.2211	0.3981	0.2302	0.2895
SF	Avg.	0.0488	0.1642	0.0574	0.1202	0.5274	1.0	0.3231	0.00	0.1944	0.2852	0.1769	0.2511
MF		0.0818	0.1702	0.1271	0.1422	0.6217	1.0	0.4445	0.00	0.4150	0.4391	0.4643	0.3949
Vpp		0.0898	0.2261	0.0988	0.1420	0.5208	1.0	0.3261	0.00	0.4767	0.4580	0.4864	0.3574
KS		0.0792	0.2524	0.1047	0.2149	0.6199	1.0	0.4167	0.00	0.1899	0.3240	0.1858	0.2954

TABLE V

USING ESTIMATED POSE [14] AND ESTIMATED SEGMENTATION [27] OR OBJECT MASKS [17] (Case IV).

while both segmentation accuracy and pose estimation affect the accuracy of semantic maps in semantic SLAM systems, the impact of segmentation accuracy far exceeds that of pose estimation and should be the focus of study within this field of research.

V. CONCLUSIONS

In this paper, we evaluated the impact of semantic segmentation and pose estimation on the semantic maps produced by class- and instance-aware dense semantic SLAM systems. We have presented this evaluation methodology in an open-format through the BenchBot framework, and encourage future research to evaluate performance using these tools. By using simulated environments to provide semantic SLAM algorithms with ground-truth pose and/or semantic segmentation data, we analyzed each component individually for different systems. In comparing the ground-truth cuboid maps with the cuboid maps extracted from the semantic SLAM systems, we have demonstrated that the largest source of error is semantic segmentation. Semantic segmentation was shown to drop mAP and OMQ performance by up to 74.3% and 71.3% respectively. It is also shown that better data association results in more accurate instance-aware maps. We also observe that providing perfect segmentation, depth and pose data alone does not guarantee perfect semantic mapping if we do not get all the objects or all the parts of the objects in the view. This aspect of SLAM, how to explore the environment to map all the objects is also important to improve the quality of semantic map. We hope that these observations will inspire or motivate further research in semantic SLAM and semantic mapping of the environment.

REFERENCES

- [1] R. F. Salas-Moreno, R. A. Newcombe, H. Strasdat, P. H. Kelly, and A. J. Davison, "SLAM++: Simultaneous Localisation and Mapping at the Level of Objects," in *IEEE CVPR*, pp. 1352–1359, 2013.
- [2] A. Rosinol, M. Abate, Y. Chang, and L. Carlone, "Kimera: an Open-Source Library for Real-Time Metric-Semantic Localization and Mapping," in *IEEE ICRA*, pp. 1689–1696, 2020.
- [3] J. McCormac, A. Handa, A. Davison, and S. Leutenegger, "SemanticFusion: Dense 3D Semantic Mapping with Convolutional Neural Networks," in *IEEE ICRA*, pp. 4628–4635, 2017.
- [4] M. Runz, M. Buffier, and L. Agapito, "MaskFusion: Real-Time Recognition, Tracking and Reconstruction of Multiple Moving Objects," in *IEEE ISMAR*, pp. 10–20, 2018.
- [5] M. Grinvald, F. Furrer, T. Novkovic, J. J. Chung, C. Cadena, R. Siegwart, and J. Nieto, "Volumetric Instance-Aware Semantic Mapping and 3D Object Discovery," *IEEE RA-L*, vol. 4, no. 3, pp. 3037–3044, 2019.
- [6] R. Hachiuma, C. Pirchheim, D. Schmalstieg, and H. Saito, "DetectFusion: Detecting and Segmenting Both Known and Unknown Dynamic Objects in Real-time SLAM," in *BMVC*, pp. 100.1–100.12, BMVA Press, 2019.
- [7] G. Narita, T. Seno, T. Ishikawa, and Y. Kaji, "PanopticFusion: Online Volumetric Semantic Mapping at the Level of Stuff and Things," in *IEEE/RSJ IROS*, pp. 4205–4212, 2019.
- [8] A. Geiger, P. Lenz, and R. Urtasun, "Are we ready for Autonomous Driving? The KITTI Vision Benchmark Suite," in *IEEE CVPR*, pp. 3354–3361, 2012.
- [9] J. Behley, M. Garbade, A. Milioto, J. Quenzel, S. Behnke, C. Stachniss, and J. Gall, "SemanticKITTI: A Dataset for Semantic Scene Understanding of LiDAR Sequences," in *IEEE/CVF ICCV*, pp. 9297–9307, 2019.
- [10] E. Kolve, R. Mottaghi, W. Han, E. VanderBilt, L. Weihs, A. Herrasti, D. Gordon, Y. Zhu, A. Gupta, and A. Farhadi, "AI2-THOR: An Interactive 3D Environment for Visual AI," *arXiv:1712.05474*, 2017.
- [11] Manolis Savva*, Abhishek Kadian*, Oleksandr Maksymets*, Y. Zhao, E. Wijmans, B. Jain, J. Straub, J. Liu, V. Koltun, J. Malik, D. Parikh, and D. Batra, "Habitat: A Platform for Embodied AI Research," in *IEEE/CVF ICCV*, pp. 9339–9347, 2019.
- [12] B. Talbot, D. Hall, H. Zhang, S. R. Bista, R. Smith, F. Dayoub, and N. Sünderhauf, "BenchBot: Evaluating Robotics Research in Photorealistic 3D Simulation and on Real Robots," *arXiv:2008.00635*, 2020. <http://benchbot.org/>, <https://github.com/qcr/benchbot>.
- [13] D. Hall, B. Talbot, S. R. Bista, H. Zhang, R. Smith, F. Dayoub, and N. Sünderhauf, "The Robotic Vision Scene Understanding Challenge," *arXiv:2009.05246*, 2020. <http://roboticvisionchallenge.org>.
- [14] T. Whelan, R. F. Salas-Moreno, B. Glocker, A. J. Davison, and S. Leutenegger, "ElasticFusion: Real-Time Dense SLAM and Light Source Estimation," *IJRR*, vol. 35, no. 14, pp. 1697–1716, Sage, 2016.
- [15] H. Oleynikova, Z. Taylor, M. Fehr, R. Siegwart, and J. Nieto, "Voxblox: Incremental 3D Euclidean Signed Distance Fields for On-Board MAV Planning," in *IEEE/RSJ IROS*, pp. 1366–1373, 2017.
- [16] J. McCormac, R. Clark, M. Bloesch, A. Davison, and S. Leutenegger, "Fusion++: Volumetric Object-Level SLAM," in *IEEE 3DV*, pp. 32–41, 2018.
- [17] K. He, G. Gkioxari, P. Dollár, and R. Girshick, "Mask R-CNN," in *IEEE ICCV*, pp. 2961–2969, 2017.
- [18] S. Yang and S. Scherer, "CubeSLAM: Monocular 3D Object SLAM," *IEEE T-RO*, vol. 35, no. 4, pp. 925–938, 2019.
- [19] L. Nicholson, M. Milford, and N. Sünderhauf, "QuadricSLAM: Dual Quadrics from Object Detections as Landmarks in Object-oriented SLAM," *IEEE RA-L*, vol. 4, no. 1, pp. 1–8, 2018.
- [20] J. Sturm, N. Engelhard, F. Endres, W. Burgard, and D. Cremers, "A Benchmark for the Evaluation of RGB-D SLAM Systems," in *IEEE/RSJ IROS*, pp. 573–580, 2012.
- [21] R. Mur-Artal and J. D. Tardós, "ORB-SLAM2: an Open-Source SLAM System for Monocular, Stereo and RGB-D Cameras," *IEEE T-RO*, vol. 33, no. 5, pp. 1255–1262, 2017.
- [22] M. Everingham, L. Van Gool, C. K. Williams, J. Winn, and A. Zisserman, "The Pascal Visual Object Classes (VOC) Challenge," *IJCV*, vol. 88, no. 2, pp. 303–338, Springer, 2010.
- [23] J. Hou, A. Dai, and M. Nießner, "3D-SIS: 3D Semantic Instance Segmentation of RGB-D Scans," in *IEEE CVPR*, pp. 4421–4430, 2019.
- [24] C. R. Qi, O. Litany, K. He, and L. J. Guibas, "Deep Hough Voting for 3D Object Detection in Point Clouds," in *IEEE/CVF ICCV*, pp. 9277–9286, 2019.
- [25] Z. Yang, Y. Sun, S. Liu, and J. Jia, "3DSSD: Point-based 3D Single Stage Object Detector," in *IEEE/CVF CVPR*, pp. 11040–11048, 2020.
- [26] D. Hall, F. Dayoub, J. Skinner, H. Zhang, D. Miller, P. Corke, G. Carneiro, A. Angelova, and N. Sünderhauf, "Probabilistic Object Detection: Definition and Evaluation," in *IEEE/CVF WACV*, pp. 1031–1040, 2020.
- [27] B. Zhou, H. Zhao, X. Puig, T. Xiao, S. Fidler, A. Barriuso, and A. Torralba, "Semantic Understanding of Scenes through the ADE20K Dataset," *IJCV*, vol. 127, no. 3, pp. 302–321, Springer, 2014.
- [28] Y. Jia, E. Shelhamer, J. Donahue, S. Karayev, J. Long, R. Girshick, S. Guadarrama, and T. Darrell, "Caffe: Convolutional Architecture for Fast Feature Embedding," in *ACM MM*, pp. 675–678, 2014.
- [29] T.-Y. Lin, M. Maire, S. Belongie, J. Hays, P. Perona, D. Ramanan, P. Dollár, and C. L. Zitnick, "Microsoft COCO: Common Objects in Context," in *ECCV*, pp. 740–755, Springer, 2014.
- [30] J. McCormac et al., "SemanticFusion Github Repository." <https://github.com/seanun163/semanticfusion> Accessed: 12-12-2020.
- [31] M. Runz et al., "MaskFusion Github Repository." <https://github.com/martinruenz/maskfusion> Accessed: 12-12-2020.
- [32] M. Grinvald et al., "Voxblox++ Github Repository." <https://github.com/ethz-asl/voxblox-plusplus> Accessed: 12-12-2020.
- [33] F. Furrer, T. Novkovic, M. Fehr, A. Gawel, M. Grinvald, T. Sattler, R. Siegwart, and J. Nieto, "Incremental Object Database: Building 3D Models from Multiple Partial Observations," in *IEEE/RSJ IROS*, pp. 6835–6842, 2018.
- [34] A. Rosinol et al., "KimeraSemantics Github Repository." <https://github.com/MIT-SPARK/Kimera-Semantics> Accessed: 12-12-2020.
- [35] Mathworks, "Matlab psegdist function." <https://au.mathworks.com/help/vision/ref/psegdist.html> Accessed: 12-12-2020.
- [36] MS COCO Team, "COCO Object Detection Evaluation." <https://cocodataset.org/#detection-eval> Accessed: 12-12-2020.